Electronic Supporting Information

A robust and porous titanium metal-organic framework for gas adsorption, CO2 capture and conversion

Xuze Pan,[a] Xuezhen Si,[a] Xiaoying zhang,[a] Qingxia Yao,*[a] Yunwu Li,[a] Wenzeng Duan,[a] Yi Qiu,*[b] Jie Su,[b] Xianqiang Huang*[a]

a. School of Chemistry and Chemical Engineering, and Shandong Provincial Key Laboratory/Collaborative Innovation Center of Chemical Energy Storage and Novel Cell Technology, Liaocheng University, Liaocheng 252000, China. E-mail: yaoqxlcu@163.com; hxqqxh2008@163.com

b. College of Chemistry and molecular engineering, Peking University, Beijing, 100871,PR China. E-mail: qiuyi@pku.edu.cn

S1 Materials and Instruments

All chemicals were commercially available and used without further purification. IR spectra were recorded on a Nicolet-iS50 FT-IR spectrophotometer with KBr pellets in the region of 4000-400 cm^{-1}. The powder X-ray diffraction (PXRD) data were collected on a Rigaku SmartLab 9 kW Advance diffractionmeter with Cu-Kα radiation (λ=1.5418 Å) at 298 K. Thermogravimetric analysis (TGA) and mass spectrum was performed under nitrogen atmosphere on a Netzsch STA 449F5-QMS403C simultaneous TG/DSC-QMS analyzer with a heating rate of 20 °C/min. N_2 and CO_2 adsorption isotherms were measured on a Micromeritics ASAP 2460 system. The sample were degassed at 150 °C for 12 h prior to the measurements. ^{1}H and ^{13}C NMR spectra were measured on Bruker 500 MHz spectrometer by using tetramethylsilane (TMS) as the internal standard. SEM-Energy-dispersive X-Ray analysis (EDX) Particle morphologies and dimensions were studied with a Thermo Fisher Scientific FIB-SEM GX4 scanning electron microscope at an accelerating voltage of 20 kV.

Table S1 The reported Ti-MOFs with various Ti-O clusters

Entry	Metalcluster/core	Materials	Surface area	Ref
1	TiO_6	ZTOF-2	S_{BET} = 1878 $m^2\ g^{-1}$	[1]
2	TiO_6	NTU-9		[2]
3	TiO_6	MIL-167		[3]
4	TiO_6	MIL-168		[3]
5	TiO_6	1-Ti		[4]
6	TiO_6	MUV-11	S_{BET} = 756 $m^2\ g^{-1}$	[5]
7	$TiO_4(\mu_2\text{-}O)_2$	ACM-1	S_{BET} = 1212 $m^2\ g^{-1}$	[6]
8	$TiO_6(\mu_2\text{-}O)$	COK-47	S_{BET} = 573 $m^2\ g^{-1}$	[7]
9	$TiO_6(\mu_2\text{-}O)$	COK-47-bdc		[7]
10	$TiO_6(\mu_2\text{-}O)$	COK-47-bpyrdc		[7]
11	$Ti(C_2O_2)_3$	Ti-CAT-5	S_{BET} = 450 $m^2\ g^{-1}$	[8]
12	Ti_2O_{11}	MIL-169		[3]
13	Ti_3O	Ti-MIL-101		[9]
14	$Ti_3(OH)_2$	Ti_3-BPDC	S_{BET} = 636 $m^2\ g^{-1}$	[10]

| 15	$Ti_3(\mu_3\text{-}O)$	COK-69	$S_{BET} = 29.13\ m^2\,g^{-1}$	[11]
16	$Ti_3(\mu_3\text{-}O)$	MIL-100(Ti)	$S_{BET} = 1321\ m^2\,g^{-1}$	[12]
17	$Co_2Ti(\mu_3\text{-}O)$	CTOF-1	$S_{BET} = 637\ m^2\,g^{-1}$	[13]
18	$Co_2Ti(\mu_3\text{-}O)$	CTOF-2	$S_{BET} = 618\ m^2\,g^{-1}$	[13]
19	$Co2Ti(\mu3\text{-}O)\ (COO)6$	PFC-20-Co_2Ti		[14]
20	$Ni2Ti(\mu3\text{-}O)\ (COO)6$	PFC-20-Ni_2Ti		[14]
21	$Mn2Ti(\mu3\text{-}O)\ (COO)6$	PFC-20-Mn_2Ti		[14]
22	$Co_2Ti(\mu_3\text{-}O)$	Co_2Ti-bdc-tpt	$S_{BET} = 1369.8\ m^2\,g^{-1}$	[15]
23	$Mg_2Ti(\mu_3\text{-}O)$	Mg_2Ti-bdc-tpt	$S_{BET} = 1460.6\ m^2\,g^{-1}$	[15]
24	$Mg_2Ti(\mu_3\text{-}O)$	Mg_2Ti-bdc-tppy	$S_{BET} = 1599.1\ m^2\,g^{-1}$	[15]
25	$Mg_2Ti(\mu_3\text{-}O)$	Mg_2Ti-bdc-tpbz	$S_{BET} = 1661.7\ m^2\,g^{-1}$	[15]
26	$Zn_3Ti(\mu_3\text{-}OH)$	ZTOF-1	$S_{BET} = 1045\ m^2\,g^{-1}$	[16]
27	$Ti_2Ca_2(\mu_3\text{-}O)_2(H_2O)_4$	MUV-10	$S_{BET} = 1041\ m^2\,g^{-1}$	[17]
28	$Ti_2Ca_2(\mu_3\text{-}O)_2(\mu_2\text{-}H_2O)_2(H_2O)_4$	LCU-402	$S_{BET} = 1460\ m^2\,g^{-1}$	This work
29	$[Ti_5(OAc)_2(OH)_6]_n$	Ti-TBP	$S_{BET} = 527.7\ m^2\,g^{-1}$	[18]
30	$(Ti_6O_9)_n$	MIL-177-HT	$S_{BET} = 690\ m^2\,g^{-1}$	[19]
31	$Ti_6(\mu_3\text{-}O)_6(\mu_3\text{-}OH)_6$	ZSTU-1	$S_{BET} = 536\ m^2\,g^{-1}$	[20]
32	$Ti_6(\mu_3\text{-}O)_6(\mu_3\text{-}OH)_6$	ZSTU-2	$S_{BET} = 628\ m^2\,g^{-1}$	[20]
33	$Ti_6(\mu_3\text{-}O)_6(\mu_3\text{-}OH)_6$	ZSTU-3	$S_{BET} = 861\ m^2\,g^{-1}$	[20]
34	Ti_6O_6	MOF-901	$S_{BET} = 550\ m^2\,g^{-1}$	[21]
35	Ti_6O_6	MOF-902	$S_{BET} = 400\ m^2 g^{-1}$	[22]
36	Ti_7O_6	PCN-22	$S_{BET} = 1284\ m^2\,g^{-1}$	[23]
37	$Ti_8O_8(OH)_4$	MIL-125	$S_{BET} = 1550\ m^2\,g^{-1}$	[24]
38	$Ti_8O_8(OH)_4$	NH_2-MIL-125	$S_{BET} = 1302\ m^2\,g^{-1}$	[25]
39	$Ti_8(\mu_2\text{-}O)_8(OAC)_8$	MIP-207	$S_{BET} = 570\ m^2\,g^{-1}$	[26]
40	$Ti_8Zr_2O_{12}$	PCN-415	$S_{BET} = 1550\ m^2\,g^{-1}$	[27]
41	$Ti_8Zr_2O_{12}$	PCN-416	$S_{BET} = 1337\ m^2\,g^{-1}$	[27]
42	$Ti_{12}O_{15}$	MIL-177-LT	$S_{BET} = 730\ m^2\,g^{-1}$	[19]
43	$Ti_n(\mu_2\text{-}O)_n$	DGIST-1	$S_{BET} = 1957.3\ m^2\,g^{-1}$	[28]
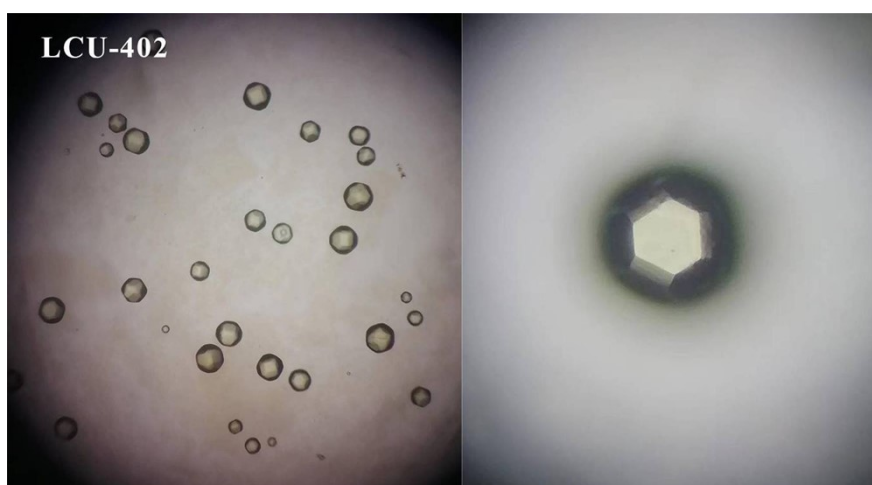
Fig. S1 Photographs of single crystals of LCU-402

S2 Scanning Electron Microscopy (SEM-EDX)

Particle morphologies, dimensions, and SEM-Energy-dispersive X-Ray analysis (EDX) of LCU-402 solids were studied with a Thermo Fisher Scientific FIB-SEM GX4 scanning electron microscope at an accelerating voltage of 20 kV. Mapping of LCU-402 showing Ti (roseo) and Ca (yellow) confirms that element distribution is homogeneous.
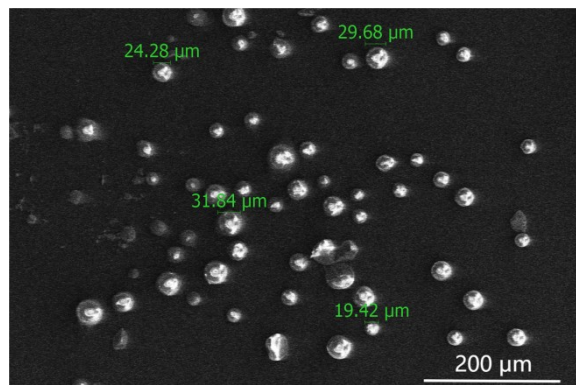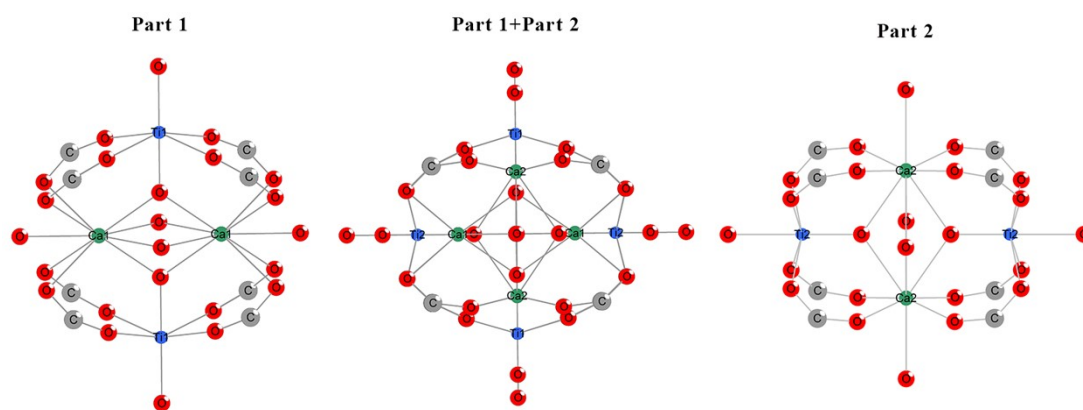

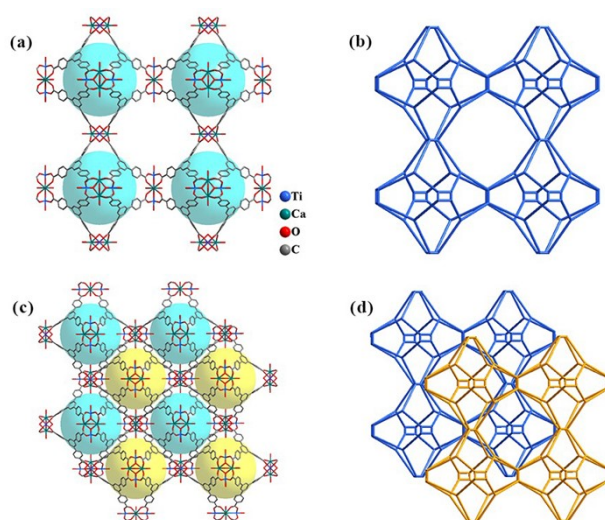**Fig. S2** Scanning Electron Microscopy (SEM) images of LCU-402.
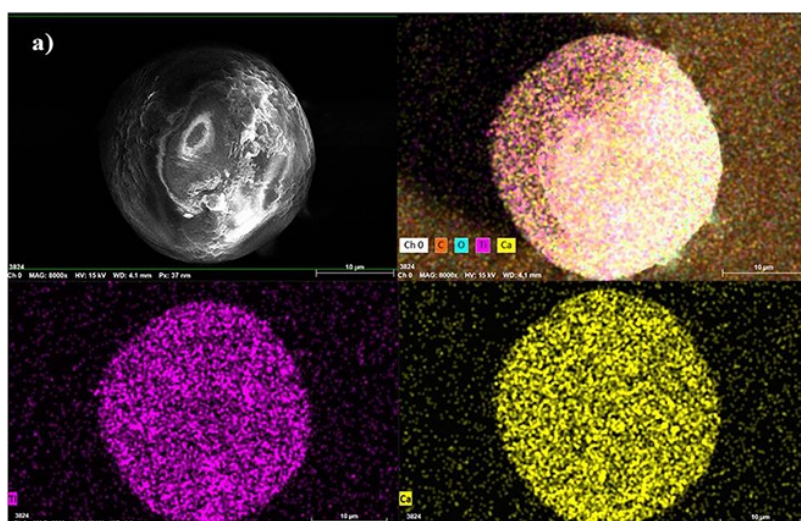
Fig. S3 Mapping of LCU-402 showing Ti (pink) and Ca (yellow)
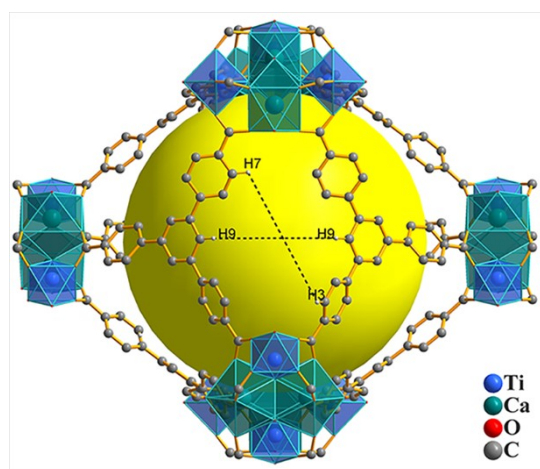
S3 Single-crystal X-ray diffraction analysis of LCU-402

Fig. S4 ORTEP representation (50% probability) of the secondary building unit showing the two fragments PART 1 and PART 2 separately.

Fig. S5 8-c SBU links 3-c BTB and (3,8)-connected augmented the net.

Fig. S6 the distance of H9···H9 and H3···H7

Table S2 Crystal data and structure refinements for LCU-402

	BTB-Ti-Ca
Empirical formula	$C_{36}H_{25.31}CaO_{11.65}Ti$
Formula weight	732.32
Crystal system	cubic
Space group	*Im-3*
a/Å	26.4097(2)
b/Å	26.4097(2)
c/Å	26.4097(2)
α/°	90
β/°	90
γ/°	90
Volume/Å^3	18420.0(4)
Z	12
ρ_{calc}g/cm^3	0.792
μ/mm^{-1}	2.215
F(000)	4518.0
2θ range for data collection/°	6.694 to 144.74
Index ranges	$-24 \leq h \leq 31$, $-31 \leq k \leq 29$, $-32 \leq l \leq 32$
GoF on F^2	1.045
Final R indexes [I>=2σ (I)]	R1 = 0.0701, wR2 = 0.2013
Final R indexes [all data]	R1 = 0.0909, wR2 = 0.2218

S4 Thermogravimetric analysis

Thermogravimetric analysis (TGA) was performed under nitrogen atmosphere on a Netzsch STA 449F5-QMS403C. TGA plot (black line) shows the LCU-402 loses all solvents (water, DMF) with a weight loss of 34.9% before 250 °C. Then, with clear plateau, it started to decompose.
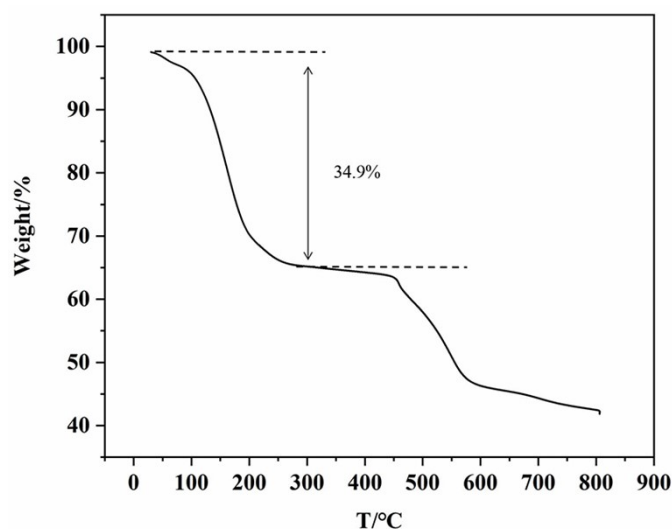

Fig. S7 TGA plot of as-synthsized LCU-402

S5 LCU-402 Pore size distribution

N_2 and CO_2 adsorption isotherms were measured on a Micromeritics ASAP 2460 system. The sample were degassed at 150 °C for 12 h prior to the measurements. Pore size distribution was analysed by using the solid density functional theory (NLDFT) for the adsorption branch assuming a cylindrical pore model.
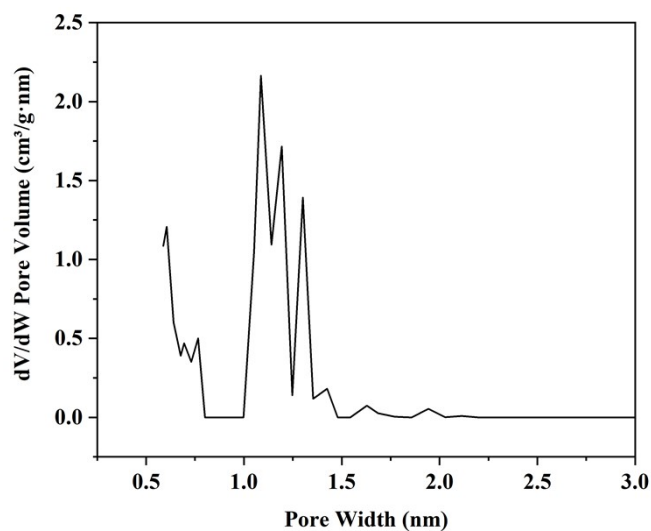

Fig. S8 LCU-402 Pore Size Distribution

S6 Isosteric heat of CO_2 adsorption (Qst)

The adsorption heat (Q_{st}) of hydrogen for the desolvated LCU-402 is fitted by Virial method using the data obtained from 273 K and 298 K with the following Equation:

$$Ln(P) = Ln(N) + \frac{1}{T}\sum_{i=0}^{m} a_i * N_i + \frac{1}{T}\sum_{j=0}^{m} a_j * N_j$$
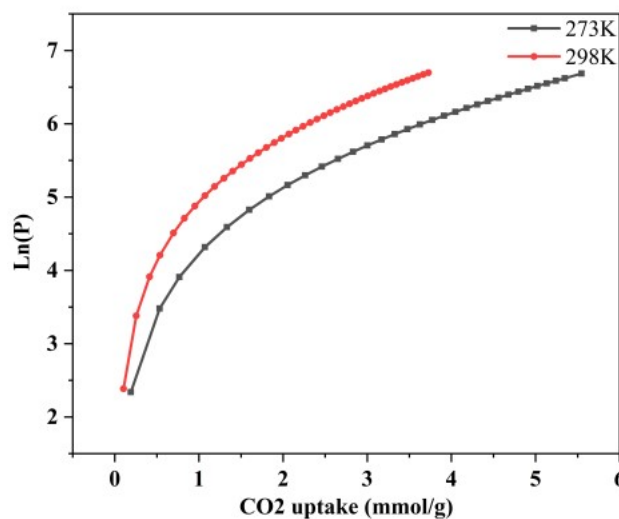
N: adsorbed quantity (mg/g);
P: pressure (mmHg);
T: temperature (K);
a_i, b_j: constant;
R: 8.314 J·mol^{-1}·K^{-1};
The isosteric enthalpy of adsorption (Q_{st}):

$$Q_{st} = Ln(P) = -R * \sum_{i=0}^{m} a_i * N_i$$

Fig. S9 Nonlinear curve fitting of CO_2 sorption isotherms for LCU-402 at 273 K and 298 K.

Table S3 Fit curve equation and factor.

		Value	Standard Error
273K	a0*	-2360.88925	11.35166
	a1*	99.60839	12.11314
	a2*	-44.62595	3.84775
	a3*	16.47407	1.47966
	a4*	-2.68098	0.29351
	a5*	0.16618	0.02099
	b0*	12.56056	0.03924
	b1*	0.08971	0.04187
	b2*	-0.02043	0.00978
	k	273	0
	a0*	-2360.88925	11.35166
	a1*	99.60839	12.11314

	a2*	-44.62595	3.84775
	a3*	16.47407	1.47966
	a4*	-2.68098	0.29351
298K	a5*	0.16618	0.02099
	b0*	12.56056	0.03924
	b1*	0.08971	0.04187
	b2*	-0.02043	0.00978
	k	298	0

$$y = Ln(x) + 1/k*(a0 + a1*x + a2*x^2 + a3*x^3 + a4*x^4 + a5*x^5) + (b0 + b1*x + b2*x^2)$$

Isosteric heat of CO_2 adsorption (Qst) was calculated by using the viral equation based on the isotherms at 273 K and 298 K.

S6 Isosteric heat of CO2 adsorption (Qst)

Isosteric heat of CO_2 adsorption (Q_{st}) was calculated by using the viral equation based on the isotherms at 273 K and 298 K.
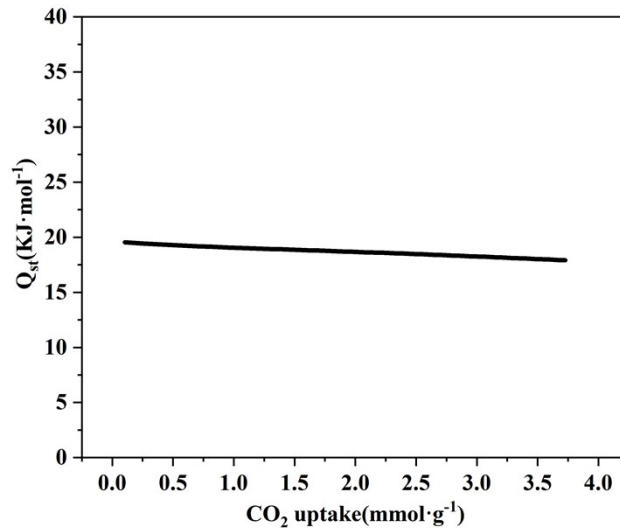
Fig. S10 Isosteric heat of adsorption (Q_{st}) calculated by the viral method

S7 IAST selectivity of LCU-402 for C_2H_6/C_2H_4 mixtures.

For adsorption isotherm data measured at 298 K, it was performed using the single point Langmuir-Freundlich isotherm model shown in Equation

$$q = q_{sat} \frac{bp^v}{1 + bp^v}$$

q: Adsorption quantity mmol/g

q_{sat} :The saturated adsorption amount of the site mmol/g

b: Single-point Langmuir-Freundlich constant of a gas component at the adsorption site kPa

V: Single-point Langmuir-Freundlich isotherm index

P: Separation pressure of the gas components kPa

Table S4 Fit curve equation and factor.

		Value	Standard Error
	A1	8.62414	0.11905
C_2H_4	B1	0.01887	2.65735E-4
	C1	0.94081	0.00909
	A1	10.13142	0.21346
C_2H_6	B1	0.02708	5.10528E-4
	C1	0.86876	0.01333

Based on the fitting parameters of the single-point Langmuir-Freundlich isotherm model at 298 K, the selectivity of LCU-402 to the C_2H_6 and C_2H_4 components was calculated using the ideal solution adsorption theory (IAST).
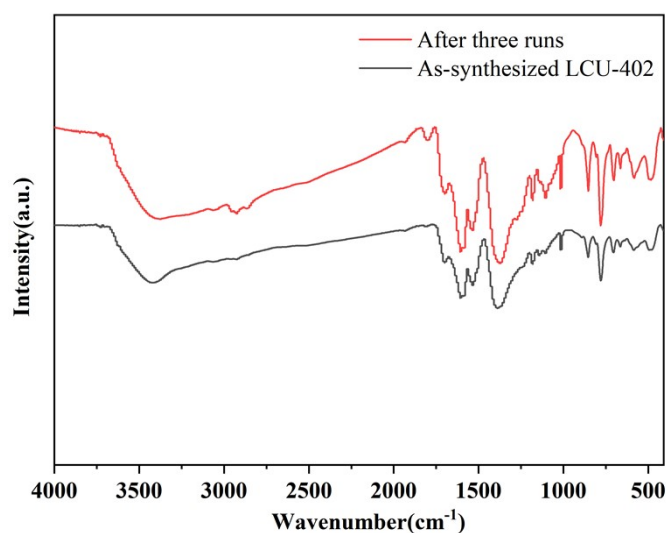
$$S_{ads} = \frac{q_1 / q_2}{y_1 / y_2}$$

S_{ads} : selectivity

q: adsorption quantity

y: molar fraction in the mixture gas

S7 Fourier-Transform infrared spectrum

Fig. S11 The FT-IR spectrum of LCU-402 as-synthesized and after three catalytic runs.

S8 Cycloaddition reaction of CO_2 with epoxides

Details of experiments and calculation procedures of catalytic efficiency:

In a typical catalytic reaction under 1 bar, epoxide (4 mmol), TBAB (1 mmol, 5 mol%), LCU-402 (0.5 mol% for open Ti sites) were put into a 15 mL Schlenk tube with solvent free environment. After centrifuging to recycle the catalyst, a little supernatant reaction mixture was taken to get analyzed by ^{1}H NMR.

The yields of propylene oxide, epichlorohydrin, epibromohydrin, 1,2-epoxyoctane, and allyl glycidyl ether (H_a for epoxides and $H_{a'}$ for carbonates, respectively) catalyzed by the LCU-402 were calculated according to the following equation.

$$Yield(\%) = \frac{I_{H_{a'}}}{I_{H_a} + I_{H_{a'}}} \times 100\%$$

The yield of styrene oxide to styrene carbonate were determined by calculation of the ^{1}H NMR integrals of corresponding highlighted protons in styrene oxide (H_a), styrene carbonate ($H_{a'}$) and phenyl group (H_b-H_f) (from styrene oxide, styrene carbonate and other by-products) according to the following equation.

$$Yield(\%) = \frac{5 \times I_{H_{a'}}}{I_{H_b - H_f}} \times 100\%$$

Figure S12. Image of the region on which EDX analysis was taken;elements ratio % from EDX analysis for organic part is represented in the table below.

Table S5 The element content determined by EDX analysis.

| Element	Atomic number	Normalized mass %	Atom %	Abs.error %
O	8	40.82	52.43	6.06
Si	14	32.96	24.12	1.39
K	19	10.74	5.65	0.48
Al	13	8.47	6.45	0.44
C	6	7.01	11.35	1.85
Ti	22	0.00	0.00	0.02
Ca	20	0.00	0.00	0.00
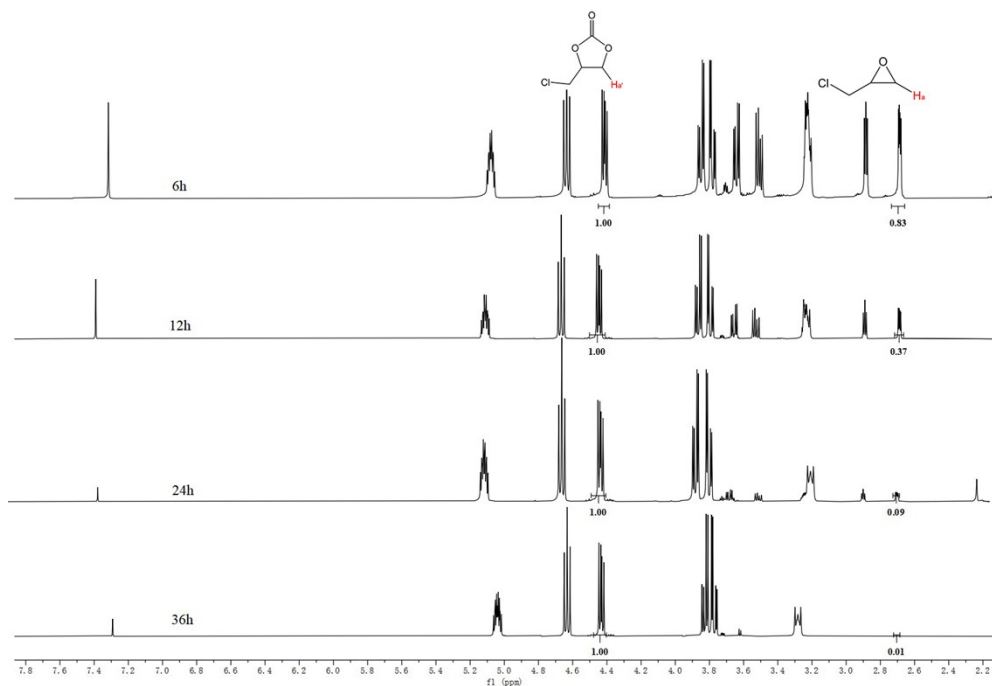
**Fig. S13** ^{1}H NMR spectrum of the mixture products under 0.15atm CO_2 atmosphere catalyzed by LCU-402 in CDCl$_3$.
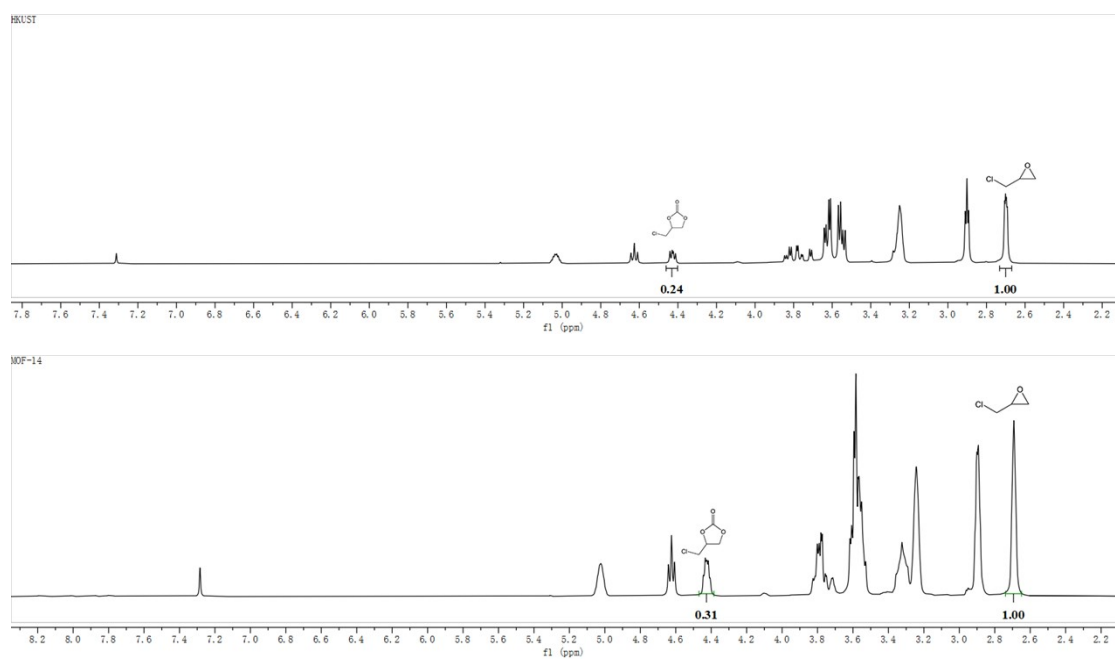
Fig. S14 ^{1}H NMR spectrum of the mixture products under 0.15atm CO_2 atmosphere catalyzed by HKUST-1 and MOF-14 in $CDCl_3$.
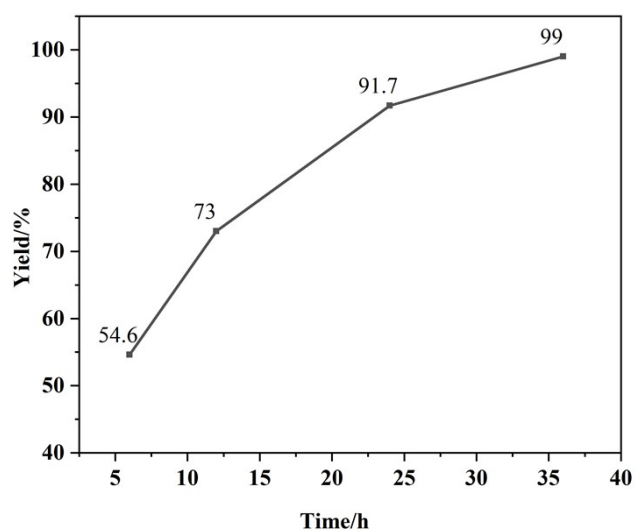
Fig. S15 Continuous sampling experiment of LCU-402 for cycloaddition reaction of epichlorohydrin with 0.15atm CO_2.
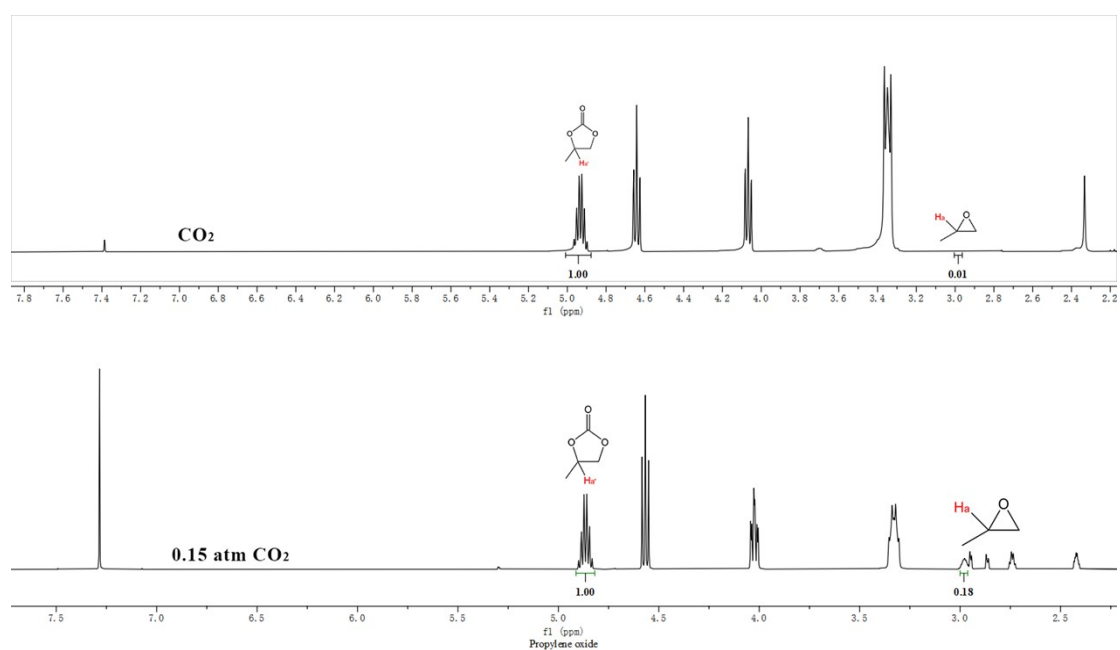
Fig. S16 ^{1}H NMR spectrum for the cycloaddition reaction of propylene epoxide under CO_2 and 0.15atm CO_2 atmosphere catalyzed by LCU-402.
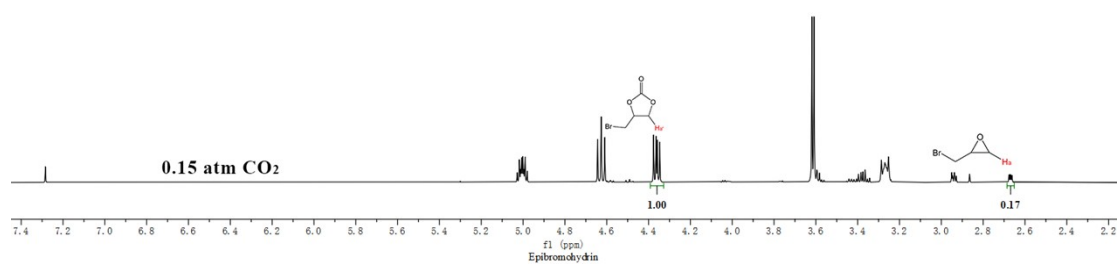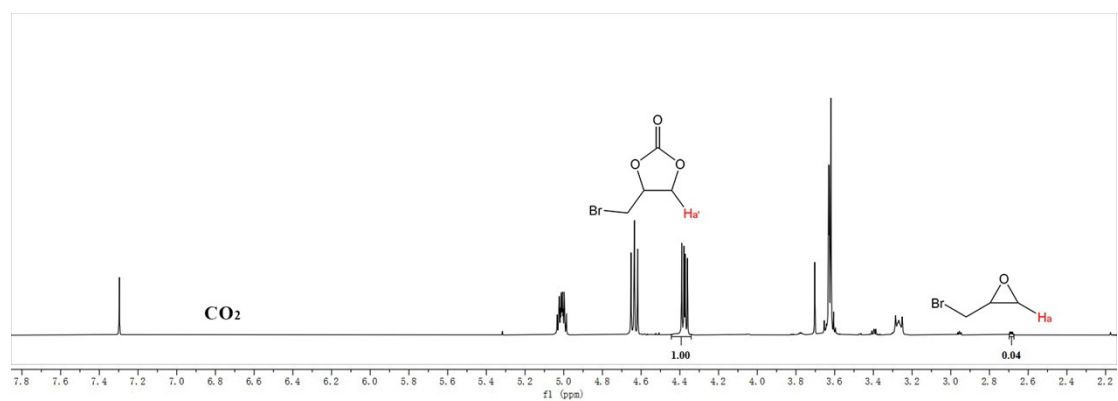
Fig. S17 ^{1}H NMR spectrum for the cycloaddition reaction of epoxy bromine propane under CO_2 and 0.15atm CO_2 atmosphere catalyzed by LCU-402.
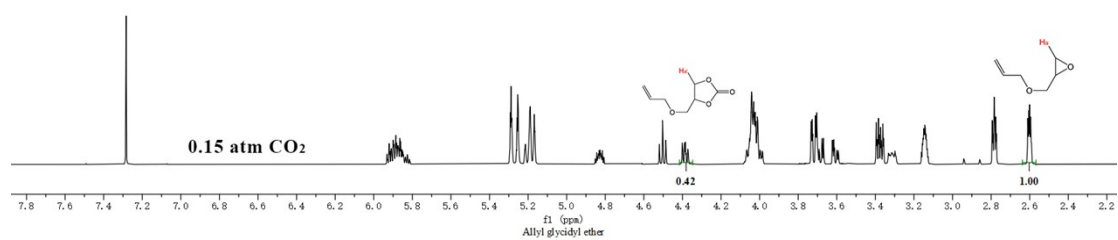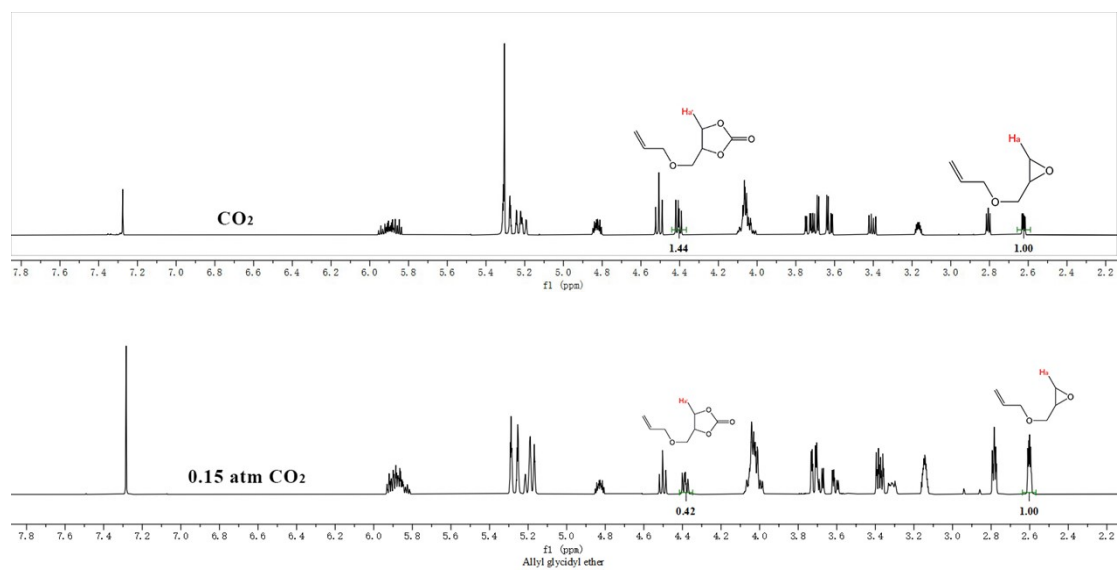
Fig. S18 ^{1}H NMR spectrum for the cycloaddition reaction of allyl glycidyl ether under CO_2 and 0.15 atm CO_2 atmosphere catalyzed by LCU-402.

Fig. S19 ^{1}H NMR spectrum for the cycloaddition reaction of cyclooxygen octane under CO_2 and 0.15 atm CO_2 atmosphere catalyzed by LCU-402.

Fig. S20 ^{1}H NMR spectrum for the cycloaddition reaction of styrene oxide under CO_2 and 0.15atm CO_2 atmosphere catalyzed by LCU-402.

Fig. S21 ^1H NMR spectrum of the mixture products under 0.15atm CO_2 atmosphere catalyzed by LCU-402 in $CDCl_3$.


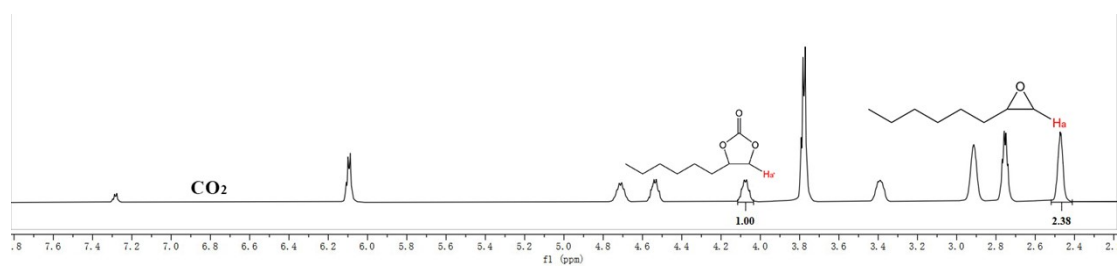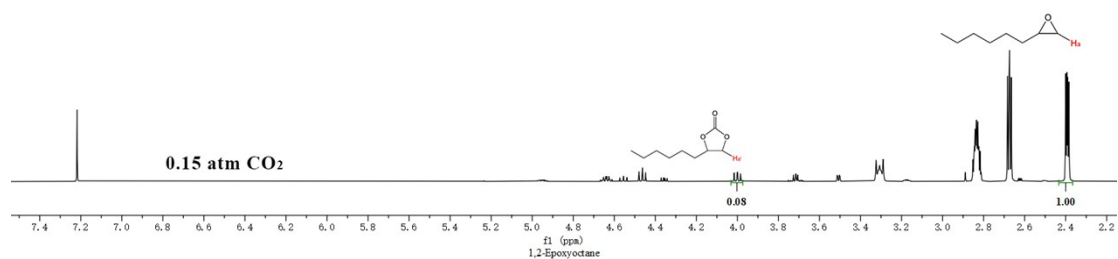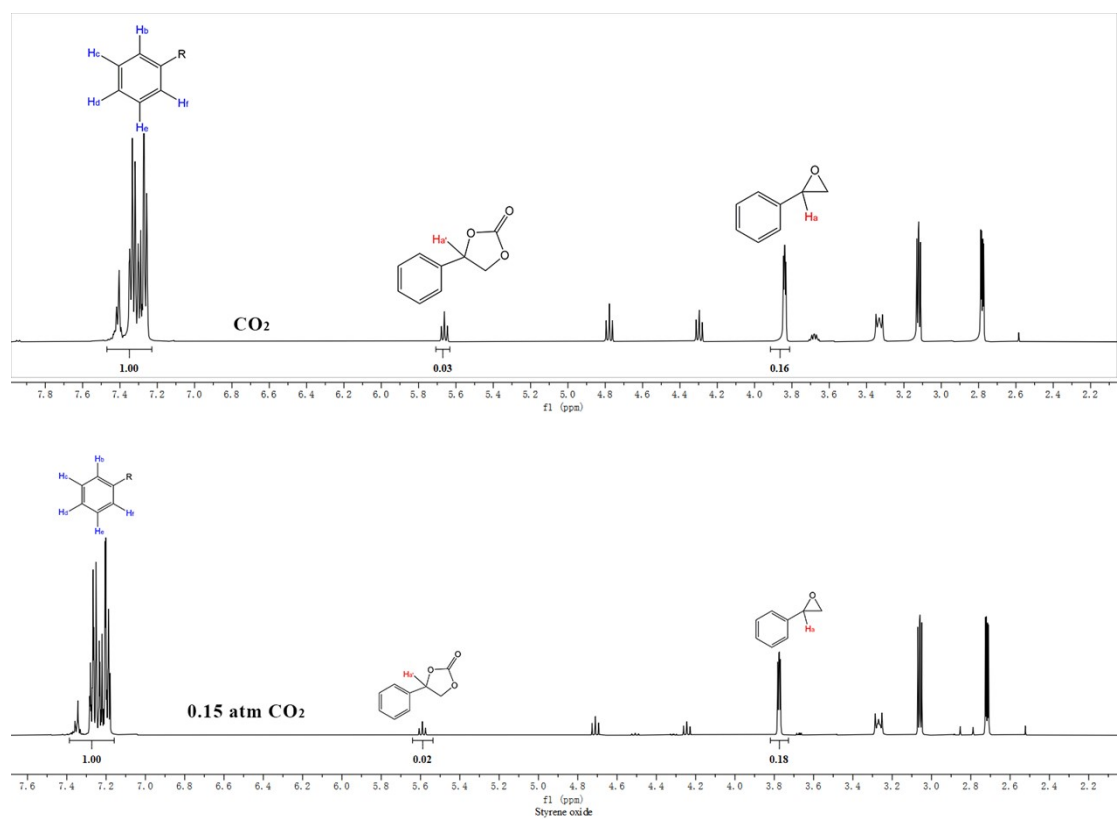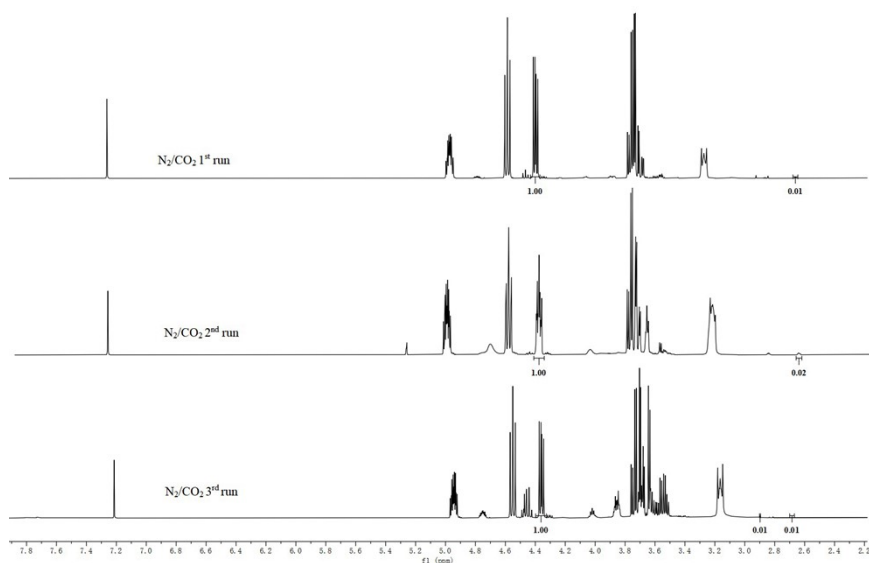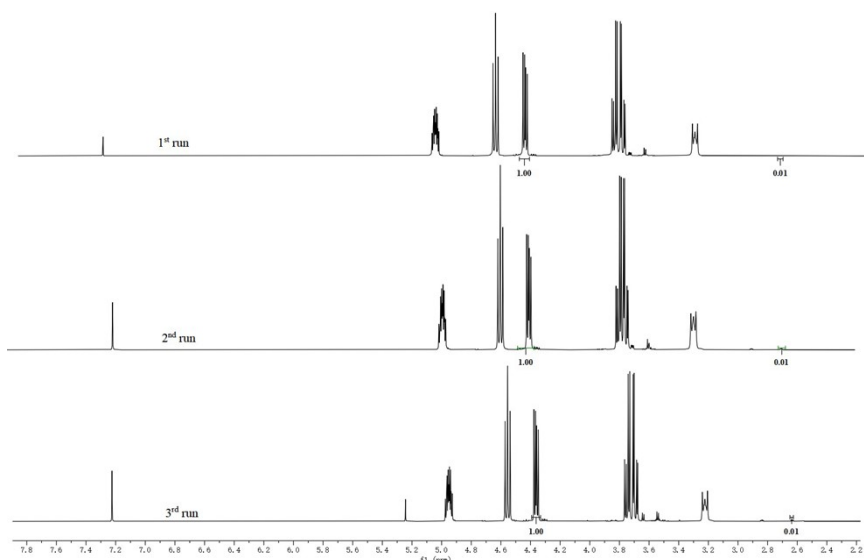**Fig. S22** ^1H NMR spectrum of the mixture products under CO_2 atmosphere catalyzed by LCU-402 in $CDCl_3$.

References

[1] K. Hong, H. Chun, Unprecedented and highly symmetric (6,8)-connected topology in a porous metal-organic framework through a Zn-Ti heterometallic approach. *Chem. Commun*., **2013**, 49, 10953

[2] J. Gao, J. Miao, P.-Z. Li, W. Y. Teng, L. Yang, Y. Zhao, B. Liu, Q. Zhang, A p-type Ti(IV)-based metal-organic framework with visible-light photo-response. *Chem. Commun*., **2014**, 50, 3786-3788.

[3] H. Assi, L. C. P. Pérez, G. Mouchaham, F. Ragon, M. Nasalevich, N. Guillou, C. Martineau, H. Chevreau, F. Kapteijn, J. Gascon, P. Fertey, E. Elkaim, C. Serre, T. Devic, Investigating the case of titanium (IV) carboxyphenolate photoactive coordination polymers. *Inorg. Chem*., **2016**, 55, 7192

[4] M. E. Ziebel, L. E. Darago, J. R. Long, Control of electronic structure and conductivity in two-dimensional metal-semiquinoid frameworks of titanium, vanadium, and chromium. *J. Am. Chem. Soc.,* **2018**, 140, 3040

[5] N. M. Padial, J. Castells-Gil, N. Almora-Barrios, M. Romero-Angel, I. d. Silva, M. Barawi, A. García-Sánchez, V. A. d. l. P. O'Shea, C. Martí-Gastaldo, Hydroxamate titanium-organic frameworks and the effect of siderophore-type linkers over their photocatalytic activity. *J. Am. Chem. Soc.,* **2019**, 141, 13124-13133.

[6] A. Cadiau, N. Kolobov, S. Srinivasan, M. G. Goesten, H. Haspel, A. V. Bavykina, M. R. Tchalala, P. Maity, A. Goryachev, A. S. Poryvaev, M. Eddaoudi, M. V. Fedin, O. F. Mohammed, J. Gascon, A titanium metal-organic framework with visible-light-responsive photocatalytic activity. *Angew. Chem. Int. Ed.*, **2020**, 59, 13468-13472.

[7] S. Smolders, T. Willhammar, A. Krajnc, K. Sentosun, M. T. Wharmby, K. A. Lomachenko, S. Bals, G. Mali, M. B. J. Roeffaers, D. E. D. Vos, B. Bueken, A titanium (IV)-based metal-organic framework featuring defect rich Ti-O sheets as an oxidative desulfurization catalyst. *Angew. Chem. Int. Ed.,* **2019**, 58, 9160-9165.

[8] N. T. T. Nguyen, H. Furukawa, F. Gandara, C. A. Trickett, H. M. Jeong, K. E. Cordova, O. M. Yaghi, Three-dimensional metal-catecholate frameworks and their ultrahigh proton conductivity. *J. Am. Chem. Soc.,* **2015**, 137, 15394-15397.

[9] J. A. Mason, L. E. Darago, W. W. Lukens, Jr, J. R. Long, Synthesis and O_2 reactivity of a titanium (III) metal-organic framework. *Inorg. Chem.*, **2015**, 54, 10096-10104.

[10] X. Feng, Y. Song, J. S. Chen, Z. Li, E. Y. Chen, M. Kaufmann, C. Wang, W. Lin, Cobalt-bridged secondary building units in a titanium metal-organic framework catalyze cascade reduction of N-heteroarenes. *Chem. Sci.*, **2019**, 10, 2193-2198.

[11] B. Bueken, F. Vermoortele, D. E. P. Vanpoucke, H. Reinsch, C.-C. Tsou, P. Valvekens, T. D. Baerdemaeker, R. Ameloot, C. E. A. Kirschhock, V. V. Speybroeck, J. M. Mayer, D. D. Vos, A flexible photoactive titanium metal-organic framework based on a $[TiIV_3(\mu_3\text{-}O)(O)_2(COO)_6]$ Cluster. *Angew. Chem. Int. Ed.*, **2015**, 127, 14118 -14123.

[12] J. Castells-Gil, N. M. Padial, N. Almora-Barrios, I. d. Silva, D. Mateo, J. Albero, H. García, C. Martí-Gastaldo, De novo synthesis of mesoporous photoactive titanium (IV)-organic frameworks with MIL-100 topology. *Chem. Sci.,* **2019**, 10, 4313-4321.

[13] K. Hong, W. Bak, D. Moon, H. Chun, Bistable and porous metal-organic frameworks with chargeneutral acs net based on heterometallic $M_3O(CO_2)_6$ building blocks. *Cryst.Growth Des.,* **2013**, 13, 4066-4070.

[14] L. Li, Z.-B. Fang, W. Deng, J.-D. Yi, R. Wang, T.-F. Liu, Precise construction of stable bimetallic metal-organic frameworks with single-site Ti (IV) incorporation in nodes for efficient photocatalytic oxygen evolution. *CCS Chem.*, **2021**, 3, 2839-2849.

[15] H. Yang, Y. Wang, R.Krishna, X. Jia, Y. Wang, A. N. Hong, C. Dang, H. E. Castillo, X. Bu, P. Feng, Pore-space-partition-enabled exceptional ethane uptake and ethane-selective ethane-ethylene separation. *J. Am. Chem. Soc.,* **2020**, 142, 2222-2227.

[16] K.Hong, W. Bak, H. Chun. Unique coordination-based heterometallic approach for the stoichiometric inclusion of high-valent metal ions in a porous metal-organic framework. *Inorg. Chem.,* **2013**, 52, 5645-5647.

[17] J. Castells-Gil, N. M. Padial, N. Almora-Barrios, J. Albero, A. R. RuizSalvador, J. Gonzlez-Platas, H. García, C. Martí-Gastaldo, Chemical engineering of photoactivity in heterometallic

titanium-organic frameworks by metal doping. *Angew. Chem. Int. Ed.,* **2018**, 57, 8453-8457.

[18] G. Lan, K. Ni, S. S. Veroneau, X. Feng, G. T. Nash, T. Luo, Z. Xu, W. Lin, Titanium-based nanoscale metal-organic framework for type I photodynamic therapy. *J. Am. Chem. Soc.,* **2019**, 141, 4204-4208.

[19] S. Wang, T. Kitao, N. Guillou, M. Wahiduzzaman, C. Martineau-Corcos, F. Nouar, A. Tissot, L. Binet, N. Ramsahye, S. Devautour-Vinot, S. Kitagawa, S. Seki, Y. Tsutsui, V. Briois, N. Steunou, G.Maurin, T. Uemura, C. Serre, A phase transformable ultrastable titanium-carboxylate framework for photoconduction. *Nat. Commun.*, **2018**, 9, 1660.

[20] C. Li, H. Xu, J. Gao, W. Du, L. Shangguan, X. Zhang, R. Lin, H. Wu,W. Zhou, Xin. Liu, J. Yao, B. Chen, Tunable titanium metal-organic frameworks with infinite 1D Ti-O rods for efficient visible-light-driven photocatalytic H_2 evolution. *J. Mater. Chem. A.*, **2019**, 7, 11928-11933.

[21] H. L. Nguyen, F. Gándara, H. Furukawa,T. L. H. Doan, K. E. Cordova, O. M. Yaghi, A titanium-organic framework as an exemplar of combining the chemistry of metal-and covalent-organic frameworks. *J. Am. Chem. Soc.*, **2016**, 138, 4330-4333.

[22] H. L. Nguyen, T. T. Vu, D. Le, T. L. H. Doan, V. Q. Nguyen, N. T. S. Phan, A titanium-organic framework: engineering of the band-gap energy for photocatalytic property enhancement. *ACS Catal.,* **2017**, 7, 338-342.

[23] S. Yuan, T.-F. Liu, D. Feng, J. Tian, K. Wang, J. Qin, Q. Zhang, Y.-P. Chen, M. Bosch, L. Zou, S. J. Teat, S. J. Dalgarno, H.-C. Zhou, A single crystalline porphyrinic titanium metal-organic framework. *Chem. Sci.,* **2015***, 6, 3926-3930.

[24] M. Dan-Hardi, C. Serre, T. Frot, L. Rozes, G. Maurin, C. Sanchez, G. Férey, A new photoactive crystalline highly porous titanium (IV) dicarboxylate. *J. Am. Chem. Soc.*, **2009**, 131, 10857-10859.

[25] Y. Fu, D. Sun, Y. Chen, R. Huang, Z. Ding, X. Fu, Z. Li An amine-functionalized titanium metal-organic framework photocatalyst with visible-light-induced activity for CO_2 reduction. *Angew. Chem. Int. Ed.*, **2012**, 51, 3364-3367.

[26] S.Wang, H. Reinsch, N. Heymans, M. Wahiduzzaman, C. Martineau-Corcos, G. De Weireld, G. Maurin, C. Serre, Toward a rational design of titanium metal-organic frameworks. *Matter,* **2020**, 2, 440.

[27] Yuan, J. S. Qin, H. Q. Xu, J. Su, D. Rossi, Y. Chen, L. Zhang, C. Lollar, Q. Wang, H. L. Jiang, D. H. Son, H. Xu, Z. Huang, X. Zou, H. C. Zhou, $[Ti_8Zr_2O_{12}(COO)_{16}]$ cluster: an ideal inorganic building unit for photoactive metal-organic frameworks. *ACS Cent. Sci.,* **2018**, 4, 105.

[28] Y. Keum, S. Park, Y.-P. Chen, J. Park, Titanium-carboxylate metal-organic framework based on an unprecedented Ti-oxo chain cluster. *Angew. Chem. Int. Ed.*, **2018**, 57,14852-14856.